Correlation between macroscopic and microscopic stress fields: Application to the 3C–SiC/Si heteroepitaxy

Massimo Camarda,[a] Ruggero Anzalone, Andrea Severino, Nicolò Piluso, Andrea Canino, Francesco La Via,[b] and Antonino La Magna
Consiglio Nazionale delle Ricerche, Istituto di Microelettronica e Microsistemi CNR-IMM, 95121 Catania, Italy

(Received 9 March 2012; accepted 10 July 2012)

In this article we develop an analytical theory that correlates the macroscopic curvature of stressed film/substrate systems with the microscopic in-plane and out-of-plane deflections of planar rotators. We have extended these stress-deflection relations in the case of nonlinear stress fields and validated the results with the aid of finite element simulations. We use this theory to study the heteroepitaxial growth of cubic silicon carbide on silicon (100) and discovered that, due to defects generated on the silicon substrate during the carbonization process, wafer curvature techniques alone may not enable determination of the stress field in the grown films either quantitatively or qualitatively.

I. INTRODUCTION

Conductive, dielectric, semiconducting, piezoelectric, and ferroelectric thin films are extensively used for micro- and nanoelectromechanical system (MEMS and NEMS) applications. One important parameter affecting the properties of MEMS and NEMS is the residual stress in the film, which can result in buckling, cracking, splintering, and sticking problems. Presently, it is very difficult to predict the residual stress from a growth process since residual stress is strongly affected by deposition conditions and subsequent fabrication processes. Stress measurement techniques are therefore essential for both process development and process monitoring. Many suggestions for stress measurements in thin films have been made over the past several decades. The conventional method involves measuring the wafer curvature to calculate the average stress using the Stoney's equation.[1–4] Other approaches use the resonant frequency technique,[5] nanoindentation,[6] x-ray diffraction (only in the case of polycrystals),[7] deflections of microstructures such as cantilevers,[8] microbridges,[9] and planar rotators (PRs)[10] or bulge tests on fabricated membranes.[11]

In general, a defective stress field $\sigma_{\mathrm{def}}(z)$, i.e., the stress related to the film/substrate interface and to defects in the system, can be represented by a polynomial expansion of the type:

$$\sigma_{\mathrm{def}}(z) = \sum_{k=0}^{\infty} \frac{\sigma_k^{\mathrm{def}}}{k!} z^k \quad , \tag{1}$$

where z is the coordinate across the thickness and σ_k^{def} is the k-order expansion around the $z = 0$ reference, which is generally chosen either located at the film/substrate interface or at the film's middle surface.

The Stoney's equation is deduced in the uniform approximation ($\sigma_0^{\mathrm{def}} \neq 0, \sigma_i^{\mathrm{def}} = 0\ \forall i > 0$):

$$\sigma_{\mathrm{def}}(z) = \sigma_0^{\mathrm{def}} \quad , \tag{2}$$

and relates the macroscopic curvature of the wafer (K_{macro}) with the defective stress[1–3]:

$$K_{\mathrm{macro}} = \frac{6 h_{\mathrm{film}}}{h_{\mathrm{sub}}^2} \frac{\sigma_0^{\mathrm{def}}}{M_{\mathrm{sub}}} \quad , \tag{3}$$

where h_{sub} and h_{film} are the thickness of the substrate and film, respectively, $M_{\mathrm{sub}} = E_{\mathrm{sub}}/(1 - \upsilon_{\mathrm{sub}})$ is the biaxial elastic modulus of the substrate, with E_{sub} and υ_{sub} being the elastic modulus and Poisson's ratio of the substrate.

On the other hand, the *residual stress*, i.e., the stress in the bowed wafer, can be determined, in the limit of the linear approximation ($\sigma_0^{\mathrm{res}} \neq 0, \sigma_1^{\mathrm{res}} \neq 0, \sigma_i^{\mathrm{res}} = 0\ \forall i > 1$) using PRs[12–14] with the following stress–displacement relations:

$$\sigma_0^{\mathrm{res}} = \frac{L_O}{2 L_C L} (M_{\mathrm{film}} \delta_x) \quad , \tag{4}$$

$$\sigma_1^{\mathrm{res}} = \frac{2}{L_C^2} (M_{\mathrm{film}} \delta_z) \quad , \tag{5}$$

where δ_x is the in-plane rotation displacement, L_{C} and L are the lengths of the indicator and test beams, respectively, L_{O} is the separation between the test beams and

[a]Address all correspondence to this author.
e-mail: massimo.camarda@imm.cnr.it
[b]This author was an editor of this focus issue during the review and decision stage. For the *JMR* policy on review and publication of manuscripts authored by editors, please refer to http://www.mrs.org/jmr-editor-manuscripts/
DOI: 10.1557/jmr.2012.264

 © Materials Research Society 2012

https://doi.org/10.1557/jmr.2012.264 Published online by Cambridge University Press

$M_{film} = E_{film}/(1 - \upsilon_{film})$ is the biaxial elastic modulus of the film. The in-plane (δ_x) and out-of-plane (δ_z) displacements of the indicator beam can be easily determined using optical or electron microscopes.

It is important to note that, when considering residual stress, the standard approximation used is the linear one, whereas, when considering the defective stress in the Stoney's equation, the uniform approximation is generally used.

The assumption of constant (linear) strain in the epilayer for the macro- and microdeflections is correct *only* when considering a fixed film thickness, but it is not correct for the prediction of the evolution of the deflections for increasing thicknesses, see, e.g., Fig. 8 in Ref. 3 or Figs. 6 and 7 in Ref. 15 for comparison with Fig. 2 of the present article.

Our goal was to correlate the "two" stresses, describe them within the same approximation and, finally, extend the analysis to any form of defective stress field.

II. CONNECTION BETWEEN MACRO- AND MICRODEFLECTIONS AND EXTENSION TO NONLINEAR STRESS FIELDS

For linking the defective and residual stress field and connecting the microdeflections (δ_x, δ_z) with the crystalline structure (i.e., with the defects), it is necessary to correlate the macro- [Eq. (3)] and micro- [Eqs. (4) and (5)] stress–displacement relations. To this end, we distinguish between the "initial stress," i.e., the stress present in the system before the relaxation, and the "final stress" as the stress after the relaxation. Consequently, the stress calculated using any type of microstructure is not the stress determined using the wafer curvature technique. In fact, this technique allows for the determination of the *defective stress* σ_{def}, i.e., the stress in the wafer before its bending, which is directly related to the defects in the system (see Fig. 1). On the other hand, the microstructures are fabricated on the bowed wafers; so they enable determination of the *residual* stress, i.e., the stress after the bending. The link between the two relaxation processes is the residual stress, which represents the final stress after the wafer bowing and the initial stress of the microbending (see Fig. 1). To simplify the description we will initially consider strain fields rather than the stress, and then later convert the strain to stress using the constitutive equation of the material (assumed linear).

In the Kirchoff's hypothesis[13] (i.e., lateral dimensions much greater than system thickness), valid both for the wafer and the microstructures as long as h_{film} is much smaller than L_{CL}, L_C, and L, we have:

$$\varepsilon_{res}(z) = \varepsilon_{def}(z) - zK_{macro} + \varepsilon_{macro} \quad , \qquad (6)$$

$$\varepsilon_{fin}(z) = \varepsilon_{res}(z) - zK_{micro} + \varepsilon_{micro} \quad , \qquad (7)$$

the macro- and microstrain (ε_{macro} and ε_{micro}) represent the in-plane relative elongation/contraction of the entire wafer (ε_{macro}) or of the microstructures (ε_{micro}), whereas K_{macro} (K_{micro}) is the curvature of the heterosystem (microstructures) (see Fig. 1). $\varepsilon_{def}(z)$ is the input function of the model and is related to the defects into the system, $\varepsilon_{res}(z)$ is the strain in the system after the bowing and $\varepsilon_{fin}(z)$ is the strain in the released microstructures that can be determined through μ-Raman analysis of the relaxed microstructures.[16]

Using the connections between macro- and microdeflections [Eqs. (6) and (7)] we can generalize Eqs. (3)–(5) by minimizing the total elastic energy of the system U (of the whole wafer and the microstructures) with respect to all the allowed macro- and microdisplacements ($K_{macro}, K_{micro}, \varepsilon_{macro}, \varepsilon_{micro}$)[17,18] (see Fig. 1).

$$U_{wafer}(\delta_{wafer}) = \int_{-h_{sub}}^{h_{film}} M\varepsilon_{res}^2(z, \delta_{wafer})dz \quad ,$$

$$U_{micro}(\delta_{micro}) = \int_{0}^{h_{film}} M\varepsilon_{fin}^2(z, \delta_{micro})dz \quad , \qquad (8)$$

where h_{sub} and h_{film} are the substrate and the film thicknesses, respectively, with the origin of the system ($z = 0$) chosen at the substrate/film interface, ($\delta_{wafer}, \delta_{micro}$) represent the macro- and microdeflections allowed consistent with the constraints in the heterosystem.

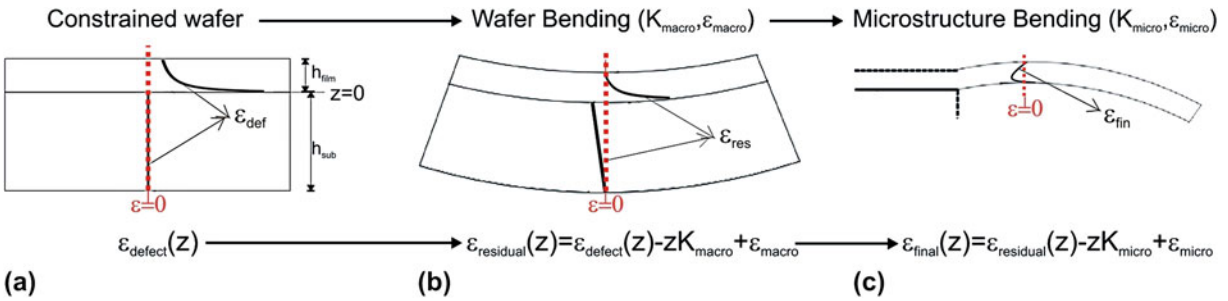


FIG. 1. Schematic modification of the internal stress field during film growth and microstructure fabrication. (a) Internal stress field of a constrained multilayered (i.e., defective or nonhomogeneous) wafer. (b) Residual stress field after wafer bending, this represents the initial stress condition of the fabricated microstructures (i.e., ε_{fin}). (c) Final strain field after microstructure (and wafer) bending.

https://doi.org/10.1557/jmr.2012.264 Published online by Cambridge University Press

M is the biaxial modulus of the substrate (for $z < 0$) and film (for $z > 0$). Note the different intervals of integration for the wafer bending ($[-h_{sub}, h_{film}]$) and the microstructures' relaxation ($[0, h_{film}]$).

The micro- and macrodeflections can be obtained by the minimization of the total elastic energy U, with respect to all the allowed displacements, i.e., by setting:

$$\left.\frac{\partial U_{wafer}}{\partial K_{macro}}\right|_{\bar{K}_{macro}} = \left.\frac{\partial U_{wafer}}{\partial \varepsilon_{macro}}\right|_{\bar{\varepsilon}_{macro}} = \left.\frac{\partial U_{micro}}{\partial K_{micro}}\right|_{\bar{K}_{micro}} = \left.\frac{\partial U_{micro}}{\partial \varepsilon_{micro}}\right|_{\bar{\varepsilon}_{micro}} = 0 \quad . \tag{9}$$

In the case of macrodeflections, we have:

$$\frac{\partial U_{wafer}}{\partial K_{macro}} = -\int_{-h_{sub}}^{h_{film}} 2Mz(\varepsilon_{def}(z) - z\bar{K}_{macro} + \bar{\varepsilon}_{macro})dz = -2\int_{-h_{sub}}^{h_{film}} Mz\varepsilon_{def}(z)dz + 2\bar{K}_{macro}\Delta_3 - 2\bar{\varepsilon}_{macro}\Delta_2 \quad ,$$

$$\frac{\partial U_{wafer}}{\partial \varepsilon_{macro}} = -\int_{-h_{sub}}^{h_{film}} 2M(\varepsilon_{def}(z) - z\bar{K}_{macro} + \bar{\varepsilon}_{macro})dz = -2\int_{-h_{sub}}^{h_{film}} M\varepsilon_{def}(z)dz + 2\bar{K}_{macro}\Delta_2 - 2\bar{\varepsilon}_{macro}\Delta_1 \quad .$$

From these relations, we can algebraically obtain $\bar{K}_{macro}$ and $\bar{\varepsilon}_{macro}$, i.e., the curvature and in-plane relative elongation/contraction of the system, as:

$$\bar{K}_{macro}\left(\frac{\Delta_2\Delta_2}{\Delta_1} - \Delta_3\right) = \frac{\Delta_2}{\Delta_1}X_1 - X_1^{'} \quad , \tag{10}$$

$$\bar{\varepsilon}_{macro}\Delta_1 = \bar{K}_{macro}\Delta_2 - X_1 \quad . \tag{11}$$

Equivalently, for the microdeflections we get:

$$\bar{K}_{micro}\left(\frac{\Theta_2\Theta_2}{\Theta_1} - \Theta_3\right) = \frac{\Theta_2}{\Theta_1}X_2 - X_2^{'} \quad , \tag{12}$$

$$\varepsilon_{micro}\Theta_1 = \bar{K}_{micro}\Theta_2 - X_2 \quad , \tag{13}$$

with:

$$\Delta_1 = M_{film}h_{film} + M_{sub}h_{sub} \qquad \Theta_1 = M_{film}h_{film} \quad ,$$

$$\Delta_2 = M_{film}h_{film}^2/2 - M_{sub}h_{sub}^2/2 \quad \Theta_2 = M_{film}h_{film}^2/2 \quad ,$$

$$\Delta_3 = M_{film}h_{film}^3/3 + M_{sub}h_{sub}^3/3 \quad \Theta_3 = M_{film}h_{film}^3/3 \quad ,$$

$$X_2 = Y_1 - \bar{K}_{macro}\Theta_2 + \bar{\varepsilon}_{macro}\Theta_1 \quad ,$$

$$X_2^{'} = Y_1^{'} - \bar{K}_{macro}\Theta_3 + \bar{\varepsilon}_{macro}\Theta_2 \quad ,$$

$$X_1 = \int_{-h_{sub}}^{h_{film}} M\varepsilon_{def}(z)dz \quad Y_1 = \int_0^{h_{film}} M_{film}\varepsilon_{def}(z)dz \quad ,$$

$$X_1^{'} = \int_{-h_{sub}}^{h_{film}} Mz\varepsilon_{def}(z)dz \quad Y_1^{'} = \int_0^{h_{film}} M_{film}z\varepsilon_{def}(z)dz \quad . \tag{14}$$

Equation (10) represents the extension of the Stoney's[1] equation valid for any film thickness (as in Ref. 2) and for *any* defective strain field $\varepsilon_{def}(z)$. Knowing $\varepsilon_{def}(z)$ or, equivalently, the initial defective stress field $\sigma_{def}(z) = \varepsilon_{def}(z)/M$, we can calculate the macro- and microdeflections of the system as:

$$\bar{K}_{macro} = \left[\frac{\Delta_2}{\Delta_1}X_1 - X_1^{'}\right] \Big/ \left(\frac{\Delta_2\Delta_2}{\Delta_1} - \Delta_3\right) \quad , \tag{15}$$

$$\delta_z = 2L^2(\bar{K}_{macro} + \bar{K}_{micro}) \quad , \tag{16}$$

$$\delta_x = \frac{2LL_C}{L_O} < \varepsilon_{fin}(z) - \varepsilon_{res}(z) > \quad . \tag{17}$$

Equation (16) has been derived noting that the out-of-plane deflection of the microstructures [either cantilever (CL) or planar rotator (PR)] is considered with respect to an ideal *flat* wafer, but not with respect to the real bowed one; hence, the *measured* microcurvature is the sum of $(\bar{K}_{macro} + \bar{K}_{micro})$. On the other hand, the test beams of the PR will elongate or contract with respect to the film/substrate stress condition (i.e., with respect to the residual stress). For this reason, the in-plane deflection, Eq. (17), is connected to the relative averaged strain $< \varepsilon_{fin}(z) - \varepsilon_{res}(z) >$ and we have:

$$\langle \varepsilon_{fin} - \varepsilon_{res} \rangle = (1/h_{film})\int_0^{h_{film}} (\varepsilon_{fin}(z) - \varepsilon_{res}(z)) = -\frac{K_{micro}h_{film}}{2} + h_{film}\varepsilon_{micro}/h_{film} = -\frac{K_{micro}h_{film}}{2} - \frac{K_{micro}\Theta_2}{\Theta_1} - X_2/\Theta_1 = -X_2/\Theta_1 \quad . \tag{18}$$

https://doi.org/10.1557/jmr.2012.264 Published online by Cambridge University Press

So, for the in-plane deflection of the PR, we finally have:

$$\begin{aligned}\delta_x &= -\frac{2LL_C}{L_O} X_2/\Theta_1 \\ &= -\frac{2LL_C}{L_O}\left[\frac{1}{h_{\text{film}}}\int_0^{h_{\text{film}}} \varepsilon_{\text{def}}(z)dz \right. \\ &\quad \left. -\frac{1}{\Theta_1}\left(\bar{K}_{\text{macro}}\Theta_2 + \bar{\varepsilon}_{\text{macro}}\Theta_1\right)\right] \quad , \end{aligned} \tag{19}$$

where the first term on the right represents the average constrained strain of the film and the second is the modification of δ_x due to the wafer bowing.

Equations (15)–(17) are valid for any defective stress field; this extension can be necessary when considering stresses in crystal whose quality (i.e., the defects density) changes substantially along the thickness. This situation occurs, among the others, in the case of heteroepitaxies characterized by large lattice mismatches such as silicon carbide on silicon epitaxy (SiC/Si)[8,19–22] or in the case of polycrystalline films where the average grain size changes, nonlinearly, along the thickness.[23] In such cases, the stress–displacement relations should be tested using the extended version of the abovementioned equations to be valid for any possible functional form of the residual stress field. The functional form that better describes the stress field for a particular growth process can then be found by means of a careful analysis of the microstructure deflections.

We have tested this theory by comparing the analytical deflections δ_x and δ_z obtained using Eqs. (19) and (16) with those obtained using finite element simulations (FESs), assuming the same functional form of the residual stress field and the same microstructure design. To test a nonlinear functional form, we used the following exponential form for the residual stress:

$$\begin{aligned}&\sigma_{\text{def}}(z) = M_{\text{film}}Ae^{-Bz} \qquad z > 0 \qquad \text{film} \quad , \\ &\sigma_{\text{def}}(z) = 0 \qquad z < 0 \qquad \text{substrate} \quad , \end{aligned} \tag{20}$$

where A and B are input parameters, to be fitted based on the observed deflections, that specify the form of the stress field along the film thickness. The analytical results have been found to be in excellent agreement with the FESs, with errors below 3%, for the entire explored range of (A, B) (corresponding to a range of δ_x, δ_z of $[-30, 30]$ and $[-150, 150]$ microns respectively, i.e., for a very large range of possible deflections).

III. MACRO- AND MICRODEFLECTIONS FOR NONDEFECTIVE SUBSTRATES

It is interesting to consider the behavior of macro- and microdeflections as functions of the film (h_{film}) and substrate (h_{sub}) thicknesses for different possible forms of the initial constrained stress field $\sigma_{\text{def}}(z)$. This study is important for at least two reasons. The first is that by studying $\delta_x(h_{\text{film}}, h_{\text{sub}})$ and $\delta_z(h_{\text{film}}, h_{\text{sub}})$, it is possible to find the most suitable fit from among the possible functional forms for $\sigma_{\text{def}}(z)$, which is a necessary step to link $\sigma_{\text{def}}(z)$ to the defects density evolution along the film thickness and in turn to the growth parameters. The second reason is technological in the sense that when the fabricated microstructures are used for sensing purposes, only specific maximum displacements are allowed for the microsensors to work properly. Indeed, the correct prediction of displacement as a function of thickness allows for the determination of a critical thickness above or below which the sensor will not work properly.

We have decided to test four different possible constrained fields; the uniform field,

$$\sigma_{\text{def}}(z) = M_{\text{film}}A \qquad z > 0 \quad , \tag{21}$$

which corresponds to the one used in the Stoney's equations[1,2]; the linear field,

$$\sigma_{\text{def}}(z) = M_{\text{film}}(A + Bz) \qquad z > 0 \quad , \tag{22}$$

that corresponds to the one used commonly to describe residual stress fields; a power law function,

$$\sigma_{\text{def}}(z) = M_{\text{film}}Az^B \qquad z > 0 \quad , \tag{23}$$

that was found to correctly describe the evolution of stacking faults film density in the heteroepitaxial growth of SiC/Si(100)[21]; and finally, an exponentially decaying function,

$$\sigma_{\text{def}}(z) = M_{\text{film}}Ae^{-Bz} \qquad z > 0 \quad , \tag{24}$$

which was found to correctly describe the evolution of the residual stress field in the GaN/Sapphire heteroepitaxy.[22]

In all the functional forms considered, A and B represent input parameters, to be fitted based on the observed deflections that describe the constrained stress field along the system thickness. In the case of uniform and linear approximation, A and B coincide with the uniform and gradient constrained strains. We can extend the concept of uniform and gradient strain/stress field in the case of nonlinear functional forms by noting that the general definition of uniform and gradient strain/stresses in the films is:

$$\sigma_{\text{uniform}} = \frac{1}{h_{\text{film}}}\int_0^{h_{\text{film}}} \sigma_{\text{res}}(z)dz \quad , \tag{25}$$

$$\sigma_{\text{gradient}} = \frac{1}{h_{\text{film}}}\int_0^{h_{\text{film}}} \frac{\partial\sigma_{\text{res}}(z)}{\partial z}dz \quad . \tag{26}$$

https://doi.org/10.1557/jmr.2012.264 Published online by Cambridge University Press

With these definitions, we can calculate the uniform and gradient stresses for any functional form considered.

We have chosen only two-parameter (A, B) functional forms to allow for a complete determination of the stress field through the two microdeflections (δ_x, δ_z). In general, for more complex functional forms (with more than two parameters), a sufficient number of measured deflections (varying, e.g., the film thickness, as was done in Ref. 24) are needed.

Finally, to allow for a consistent application of these different functional forms, we have chosen (A, B) for obtaining the following fixed values: $\delta_z = -24\,\mu\text{m}$ and $\delta_x = 3.2\,\mu\text{m}$ at $h_{\text{film}} = 2.34\,\mu\text{m}$ for all the considered functional forms. These specific microdeflections have been found in the heteroepitaxial growth of 3C–SiC/Si(100).[10,26] As can be seen in Figs. 2, 3, and 4, the four functional forms give rise to quite different results. Specifically, the out-of-plane deflection is the perfect probe to distinguish between linear and nonlinear constrained stress fields, as seen in Fig. 4. In the case of linear constrained fields, δ_z is independent of h_{film} (and equal to zero in the uniform case). This is not what was found in the case of the heteroepitaxy of 3C–SiC/Si(100).[10,25] This means that, in this specific growth, the constrained stress field in the film is nonlinear.

It is also interesting to note that in the case of linear approximation, and with the chosen parameters, there is an inversion of the wafer curvature (from concave to convex) for $h_{\text{film}} \sim 3\,\mu\text{m}$. This is the result of a self-compensation of the stress field inside the film. In other words, at $h_{\text{film}} \sim 3\,\mu\text{m}$, $\int_0^{h_{\text{film}}} \sigma_{\text{def}}(z)dz = 0$ so that we get $K_{\text{macro}} = \delta_x = 0$. This phenomenon can indeed be present in highly defective growths for which the wafer bending can be reversed for specific values of film thickness [see Fig. 2(b) in Ref. 26].

Note that in these conditions, the wafer can be flat even in the presence of highly stressed films. These particular conditions can be identified either by careful analysis of the out-of-plane deflections (which will be different from zero, expected in the case of an unstressed film) or through confocal μ-Raman analysis that enables investigation of the residual stress field along the film thickness (see Fig. 5 and Ref. 27).

Finally, as can be seen in the insets of Figs. 3 and 4, the power law function has a much stronger dependency on h_{film} for $h_{\text{film}} \to 0$ than the exponential function. For this reason, a careful analysis of either δ_x or δ_z for thin films ($h_{\text{film}} \sim 1\,\mu\text{m}$) would enable identification of the nonlinear functional form that better describes the constrained stress in the film. Finally, it is interesting to consider the initial (defective) [Eq. (6)] and final stress fields [Eq. (7)] in the

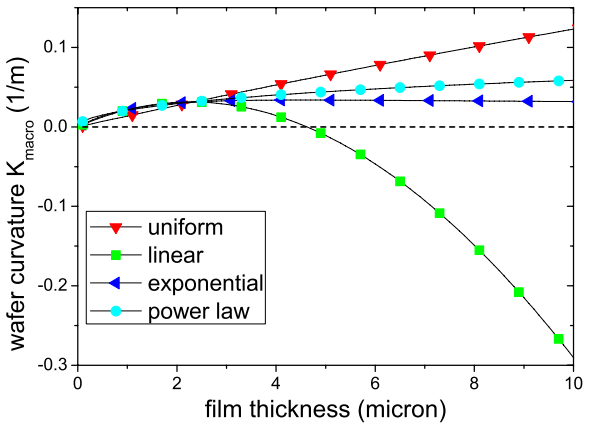


FIG. 2. Wafer curvature as a function of film thickness in the pure uniform, linear, power law and exponential approximations. Assuming no constrained stress in the substrate. ε_0 and ε_1, for each fitting function, were chosen so that $\delta_z(h = 2.34\,\mu\text{m}) = -24\,\mu\text{m}$ and $\delta_x(h = 2.34\,\mu\text{m}) = 3.2\,\mu\text{m}$, consistent with the observed deflections in microstructures in the SiC/Si(100) hetero system.[10,25] The geometrical parameters of the wafer and microstructures considered are: $L_O = 20\,\mu\text{m}$, $L = 300\,\mu\text{m}$, $L_{CL} = 400\,\mu\text{m}$, $L_C = 160\,\mu\text{m}$, $w = 10\,\mu\text{m}$, $h_{\text{film}} = 2.34\,\mu\text{m}$, and $h_{\text{sub}} = 525\,\mu\text{m}$.

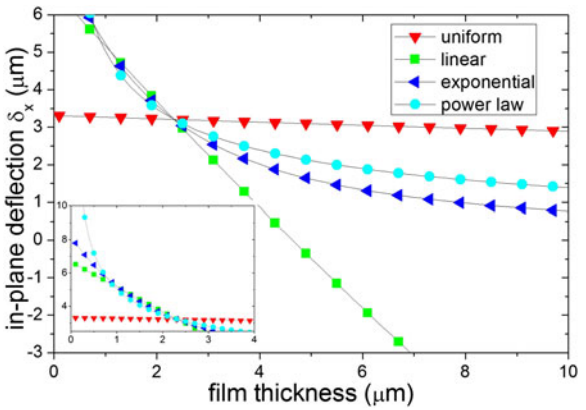


FIG. 3. Dependency of the in-plane rotation as a function of film thickness in the pure uniform, linear, power law and exponential approximations. Inset highlights the rotation for thin films. Same parameters used as in Fig. 2.

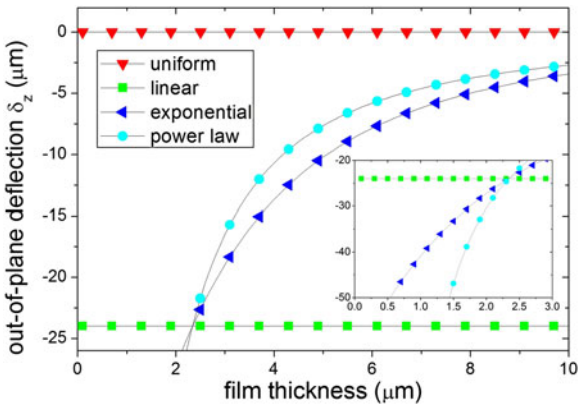


FIG. 4. Dependency of the out-of-plane deflection as a function of film thickness in the pure uniform, linear, power law and exponential approximations. Inset highlights the deflection for thin films. Same parameters used as in Fig. 2.

https://doi.org/10.1557/jmr.2012.264 Published online by Cambridge University Press

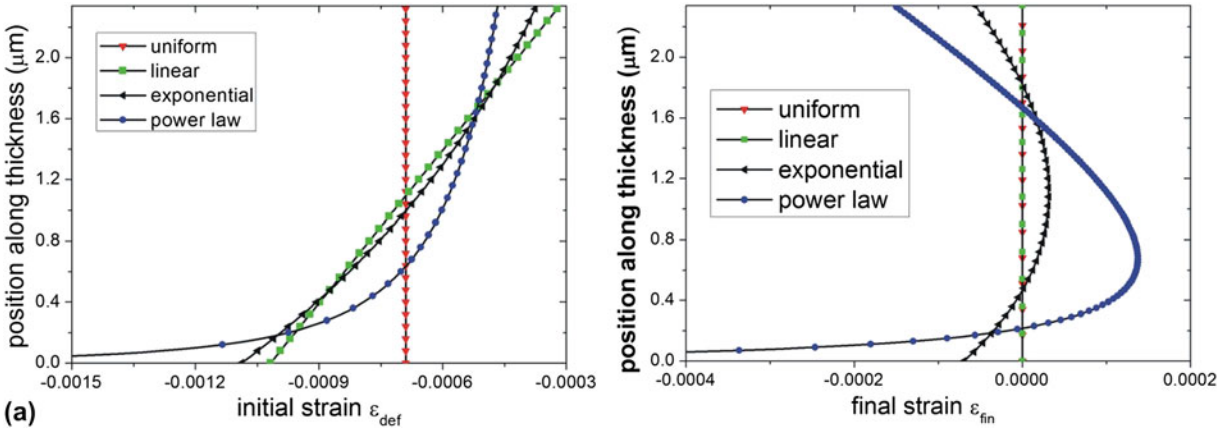


FIG. 5. Defective, $\varepsilon_{def}(z)$, (a) and final $\varepsilon_{fin}(z)$ (b) strain fields along the film thickness. As can be seen, only nonlinear constrained fields give rise to nonzero final strains in the Kirchhoff's hypothesis; on the other hand, all functional forms considered give rise to a zero final average strain $<\varepsilon_{fin}>$. Calculation parameters are the same as in Fig. 2.

case of the four functional forms considered. As can be seen in Fig. 5, only exponential and power law functional forms (i.e., nonlinear functional forms) give rise to nonzero final stress fields. This situation can easily be identified by confocal μ-Raman analysis of the released microstructures.

IV. MACRO- AND MICRODEFLECTIONS FOR DEFECTIVE SUBSTRATES

It is important to note that for all the considered functional forms [Eqs. (21)–(24)], we have assumed $\sigma_{def}(z) = 0$ in the substrate ($z < 0$). This assumption might not be valid for those heterogrowths where the substrate crystalline structure changes during the deposition of the film, i.e., where defects are generated in the substrate during the growth process. We will now consider this important case.

For studying the modifications caused by a constrained stress field located in the substrate, we start by considering the product $\alpha = K_{macro}\delta_x$ as a function of the film thickness and film stress. In the case of nondefective substrates, α is always greater than zero for all considered thicknesses (h_{film}, h_{sub}) and for all constrained functional forms [Eqs. (21)–(24)]. This is related to the assumption, which is generally correct, that a tensile (compressive) stress results in a concave (convex) wafer bending[1–3] and in a positive (negative) PR deflection.[12] In other words, when $\sigma_{def}(z<0) = 0$, the curvature of wafer and the in-plane deflection of the PR are tightly connected, and both are a direct indication of the stress status of the film [i.e., of the average constrained stress in the film; see Eq. (19)]. These results change when $\sigma_{def}(z<0) \neq 0$. To study this problem, we reconsidered the four constrained fields, Eqs. (21)–(24), and included a constant strain opposite to that present in the film and located in the substrate near the heterointerface:

$$\varepsilon_{def}(z) = -0.0005 \qquad -h_{SubDefect} < z < 0\,\mu m \quad , \quad (27)$$

with $h_{SubDefect} = 2\,\mu m$. As can be seen in Fig. 6(a), in this condition, α can be either positive or negative depending on the film thickness. This means that, in these circumstances, a tensile (compressive) film can be associated with a convex (concave) wafer bow [Fig. 6(b)] and that standard stress analysis based on wafer curvature analysis (Stoney's equation and related issues[1–3]) would fail to predict the stress field of the film correctly. As an example, it can happen that $K_{macro} = 0$ (no wafer bow) even if the film is under a high stress condition or tensile stress and the wafer curvature is convex [see Fig. 6(b)]. This particular situation can be identified by either Raman spectroscopy or x-ray diffraction (XRD) of the unreleased film or by analysis of the microstructure deflections. It is important to note that this situation is different from the "self-compensation" of the stress field considered in the previous section. In fact, in that case, a flat wafer ($K_{macro} = 0$) is always associated with a $\delta_x = 0$ in-plane deflection of the PR (see Fig. 3), i.e., in the case of "self-compensation" the tight link between K_{macro} and δ_x is preserved. In the case of defective substrates, on the other hand, this connection is lost, so that we can have $K_{macro} = 0$ and $\delta_x \neq 0$. In such cases, only δ_x, not the macroscopic bending, allows to identify the type of stress (tensile or compressive) in the epilayer correctly. It is noteworthy that in both situations, the rear of the substrate acts as an elastic constraint hindering the bowing of the system. For this reason, thicker substrates will always result in bow reduction. On the other hand, when $\int \varepsilon_{def}(z)dz = 0$, $K_{macro} = 0$ independently of the substrate thickness. This "compensated" stress condition can be important in subsequent wafer processes (backside thinning).

https://doi.org/10.1557/jmr.2012.264 Published online by Cambridge University Press

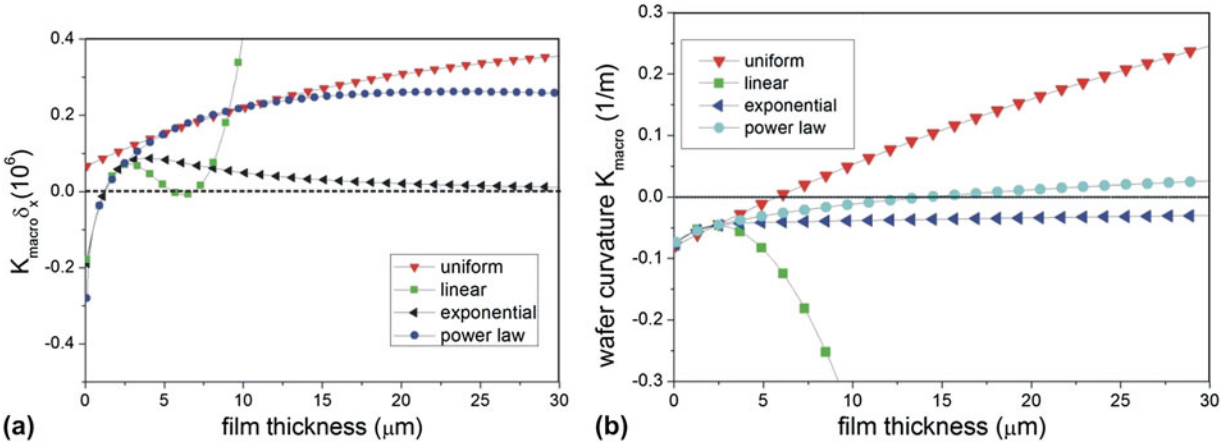


FIG. 6. (a) $\alpha = K_{macro}\delta_x$ and (b) Wafer curvature, as a function of the film thickness in the case of a defective substrate [$\sigma_{def}(-h_{SubDefect} < z < 0) = -0.001$], with $h_{SubDefect} = 2\,\mu m$. Calculation parameters are the same as in Fig. 2. In all functional forms considered, the average film stress is tensile (except the linear form for $h_{film} > 3\,\mu m$, see Fig. 5).

V. ANALYSIS OF THE EXPERIMENTAL RESULTS ON THE HETEROEPITAXIAL GROWTH OF 3C–SiC ON Si(100)

Based on these considerations, we have studied the heteroepitaxial chemical vapor deposition (CVD) growth of single-crystal cubic silicon carbide (3C–SiC) on silicon (100). The growth consisted mainly of two different steps, namely, an initial "carbonization" of the silicon surface followed by the growth.

During carbonization, propane (C_3H_8) and hydrogen (H_2) flow through the reactor while the temperature is ramped to 1135 °C at a process pressure of ~400 Torr. Once the temperature stabilizes, the wafer is held under a steady-state condition of gas flow, temperature, and pressure for 4 min. This allows the conversion of the Si wafer surface to a 3C–SiC buffer layer (carbonization).

After the 4-min carbonization plateau, the growth phase began. Silane (SiH_4) was then introduced into the gas stream; the temperature was ramped to 1370 °C while the process pressure was maintained at 400 Torr. The growth rate and thickness were set equal to 2.45 μm/h and $h_{film} = 2.4\,\mu m$, respectively at the wafer center. The grown film was analyzed through optical profilometer, confocal μ-Raman, and microstructure deflections. As can be seen in Table I, there is an inconsistency between the wafer curvature analysis and the other techniques used, specifically: confocal μ-Raman and PR deflections indicate a tensile residual film stress, whereas the convex wafer bow would indicate a film under compressive stress.[1–3] In other words, there is a clear inconsistency between wafer curvature techniques and the other analyses (Raman and microstructure). This inconsistency, based on the results of the previous section, could be the result of a constrained stress generated in the silicon substrate during the growth process. Indeed, it is well known that during the "carbonization" step, several defects are generated underneath the interface between the 3C–SiC and the silicon substrate.[28–30] But these defects were not expected to play a central role in the deformation of the wafer, i.e., it was not expected that the dominant cause of the wafer bending were the defects in the substrate. In these conditions, wafer curvature analyses are not a reliable technique for the determination of the correct film stress field. To further investigate this hypothesis we have analyzed several 3C/Si samples, both on silicon (111) and (100), through cross-sectional μ-Raman to identify the stress status of the substrate throughout the entire thickness. As can be clearly seen in Fig. 7, the Raman shift associated with the silicon peak increases toward higher frequencies close to the SiC/Si interface, experimentally confirming the existence of such compressed region within the substrate. Note also that the linear trend of the Raman shift (and, thus, of the strain[16,27]) far from the interface ($z < -200$ μm), represents the defect-free region of the substrate, from this linear trend we can also extract the curvature of the wafer, in fact in this region we have $\varepsilon_{res}(z) = -zK_{macro} + \varepsilon_{macro}$, being $\varepsilon_{def}(z) = 0$, so that $K_{macro} = -\partial\varepsilon_{res}(z)/\partial z$. It has to been noted that it was not possible to obtain such cross-section in the same epiwafer considered for the microstructures because the film was too thin to avoid delamination during cross-section preparation.

TABLE I. Results of the analysis of a 3C–SiC/Si(100) epitaxially grown film. The grown film was analyzed through optical profilometer, confocal μ-Raman, and microstructure deflections. Second line shows the type of stress in the film as deduced by the analysis.

h_{epi} (μm)	K_{macro} (1/m)	LO Raman (cm^{-1})	TO Raman (cm^{-1})	δ_x
2.34	−0.08	971.58 ± 0.1	795.6 ± 0.1	3.2 ± 0.1 μm
	Compressive[1–3]	Tensile[11]	Tensile[11]	Tensile[10,12]

https://doi.org/10.1557/jmr.2012.264 Published online by Cambridge University Press

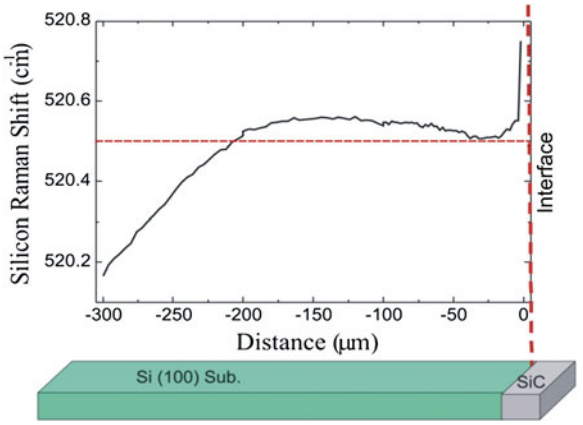


FIG. 7. Cross-sectional μ-Raman analysis of a 15-μm SiC/Si(100) film with concave curvature, consistent with Fig. 6(b). Red dashed line shows the stress free Raman shift value.

Finally, as a further confirmation of this interpretation, it is interesting to consider the dependency of K_{macro} on h_{film} for this film. As can be seen in Fig. 6(b), for $h_{\text{film}} < \bar{h}_{\text{inv}}$ (with $\bar{h}_{\text{inv}}$ depending on the chosen functional form), the curvature is a *decreasing* function of the film thickness in contrast to the usual dependency.[1–3] Specifically, for $h_{\text{film}} = \bar{h}_{\text{inv}}$, there is equilibrium of the stresses, i.e., $\int_0^{h_{\text{film}}} \sigma_{\text{def}}(z)dz = -\int_{-h_{\text{sub}}}^{0} \sigma_{\text{def}}(z)dz$ so that we get $K_{\text{macro}} = 0$ (and $\delta_x \neq 0$). This is, indeed, what was found in Ref. 27.

Finally, it is important to note that the inversion of the curvature has been found also by varying the preparation of the substrate[31–33] or tuning of the carbonization step.[34] These results could be related to a different defect inclusion in the silicon substrate rather than to a change in the film microstructure. Unfortunately, the literature data do not specifically focus on the mechanical or structural analysis (e.g., determination of the Young's modulus, strain status, or crystalline quality) of the substrate, this prevents further quantitative comparisons in the framework of the presented model.

VI. CONCLUSIONS

The aim of this work was to achieve a consistent methodology for the stress/strain analysis based on the fabrication of microstructure probes. In particular, we have developed a systematic approach to correlate global (wafer-scale) measurements to those obtained by local indicators (such as cantilevers or planar rotators) of the strain status. Our interest is to push the analysis capability in case of extreme conditions of strongly nonlinear dependence of the local strain field on some material coordinate (e.g., the thickness of the grown epitaxial layer). In this case, a nontrivial relationship occurs between the measurable quantities (deflections and curvatures) and the strain field of the system in study.

We have derived the analytical relationships linking macroscopic and microscopic observables by formally decoupling the sequences of relaxation steps. The derived formulas have been tested in detail using numerical finite element simulations, which demonstrate the reliability of our method. The application of our formalism is useful to understand some apparent discrepancies between the measured values of macro- and microparameters in practical cases. The analysis of a particular case study on the heteroepitaxial growth of 3C–SiC on Si(100) shows that these apparent discrepancies are the signature of a complex relaxation mechanism, and an accurate data interpretation gives important insights into the microstructural configuration of the samples under study.

REFERENCES

1. G.G. Stoney: The tension of metallic films deposited by electrolysis. *Proc. R. Soc. London, Ser. A* **172**, 82 (1909).
2. C.A. Klein: How accurate are Stoney's equations and recent modifications. *J. Appl. Phys.* **88**, 5487 (2000).
3. G.C.A.M. Janssen, M.M. Abdalla, F. van Keulen, B.R. Pujada, and B. van Venrooy: Celebrating the 100th anniversary of the Stoney's equation for film stress: Developments from polycrystalline steel strips to single crystal silicon wafers. *Thin Solid Films* **517**, 1858 (2009).
4. L.B. Freund: The stress distribution and curvature of a general compositionally graded semiconductor layer. *J. Cryst. Growth* **132**, 341 (1993).
5. T. Ikeharal, R.A.F. Zwijze, and K. Ikeda: New method for an accurate determination of residual strain in polycrystalline silicon films by analyzing resonant frequencies of micromachined beams. *J. Micromech. Microeng.* **11**, 55 (2001).
6. S. Sureh and A.E. Giannakopoulos: A new method for estimating residual stresses by instrumented sharp indentation. *Acta Mater.* **46**, 5755 (1998).
7. U. Welzel, J. Ligot, P. Lamparter, A.C. Vermeulen, and E.J. Mittemeijer: Solidification microstructures: Recent developments and future directions. *J. Appl. Crystallogr.* **38**, 1 (2005).
8. R. Anzalone, M. Camarda, C. Locke, D. Alquier, A. Severino, M. Italia, D. Rodilosso, C. Tringali, A. La Magna, G. Foti, S.E. Saddow, F. La Via, and G. D'Arrigo: Low stress heteroepitaxial 3C-SiC films characterized by microstructure fabrication and finite elements analysis. *J. Electrochem. Soc.* **157**, H438–H442 (2010).
9. H. Guckel, T. Randazzo, and D.W. Burns: A simple technique for the determination of mechanical strain in thin films with applications to polysilicon. *J. Appl. Phys.* **57**, 1671 (1985).
10. R. Anzalone, G. D'Arrigo, M. Camarda, C. Locke, S.E. Saddow, and F. La Via: Advanced residual stress analysis and FEM simulation on heteroepitaxial 3C-SiC for MEMS application. *J. Micromech. Syst.* **20**, 745 (2011).
11. S. Rohmfeld, M. Hundhausen, L. Ley, C.A. Zorman, and M. Mehregany: Quantitative evaluation of biaxial strain in epitaxial 3C-SiC layers on Si(100) substrates by Raman spectroscopy. *J. Appl. Phys.* **91**, 1113 (2002).
12. B.P. Drieenhuizen, J.F.L. Goosen, P.J. French, and R.F. Wolffenbuttel: Comparison of techniques for measuring both compressive and tensile stress in thin films. *Sens. Actuators, A* **37–38**, 756–765 (1993).
13. S. Timoshenko and S. Woinowsky-Krieger: *Theory of Plates and Shells* (McGraw-Hill, New York, 1959).
14. M. Camarda, R. Anzalone, A. Severino, N. Piluso, A. La Magna, and F. La Via: Complete determination of the local stress field in epitaxial thin films using single microstructure. *Mater. Sci. Forum* **679**, 213 (2011).

https://doi.org/10.1557/jmr.2012.264 Published online by Cambridge University Press

15. S.N.G. Chu: Elastic bending of semiconductor wafer revisited and comments on Stoney's equation. *J. Electrochem. Soc.* **145**, 3621 (1998).
16. N. Piluso, M. Camarda, R. Anzalone, A. Severino, A. La Magna, G. D'arrigo, and F. La Via: Raman stress characterization of heteroepitaxial 3C-SiC free standing structures. *Mater. Sci. Forum* **679**, 141 (2011).
17. S. Huang and X. Zhang: Extension of the Stoney's formula for film-substrate systems with gradient stress for MEMS applications. *J. Micromech. Microeng.* **16**, 382–389 (2006).
18. N.J. Salamon and C.B. Masters: Bifurcation in isotropic thin film/substrate plates. *Int. J. Solids Struct.* **32**, 473 (1995).
19. A. Severino, C. Bongiorno, N. Piluso, M. Italia, M. Camarda, M. Mauceri, G. Condorelli, M.A. Di Stefano, B. Cafra, A. La Magna, and F. La Via: High-quality 6 inch (111) 3C–SiC films grown on off-axis (111) Si substrates. *Thin Solid films* **518**, s165 (2010).
20. A. Severino, M. Camarda, S. Scalese, P. Fiorenza, S. Di Franco, C. Bongiorno, A. La Magna, and F. La Via: Preferential oxidation of stacking faults in epitaxial off-axis (111) 3C-SiC films. *Appl. Phys. Lett.* **95**, 111905 (2009).
21. M. Zielinski, M. Portail, S. Roy, T. Chassagne, C. Moisson, S. Kret, and Y. Cordier: Elaboration of (1 1 1) oriented 3C-SiC/Si layers for template application in nitride epitaxy. *Mater. Sci. Eng., B* **165**, 9–14 (2009).
22. H. Siegle, A. Hoffmann, L. Eckey, C. Thomsen, J. Christen, F. Bertram, D. Schmidt, D. Rudloff, and K. Hiramatsu: Vertical strain and doping gradients in thick GaN layers. *Appl. Phys. Lett.* **71**, 2490 (1997).
23. R. Anzalone, M. Camarda, D. Alquier, M. Italia, A. Severino, N. Piluso, A. La Magna, G. Foti, C. Locke, S.E. Saddow, A. Roncaglia, F. Mancarella, A. Poggi, G. D'Arrigo, and F. La Via: Residual stress measurement and simulation of 3C-SiC single and poly crystal cantilevers. *Mater. Sci. Forum* **645**, 865 (2010).
24. S. Seok, B. Lee, and K. Chun: A new electrical residual stress characterization using bent beam actuators. *J. Micromech. Microeng.* **12**, 562 (2002).
25. R. Anzalone, M. Camarda, G. D'Arrigo, C. Locke, A. Canino, N. Piluso, A. Severino, A. La Magna, S.E. Saddow, and F. La Via: Advanced stress analysis by microstructures realization on high quality heteroepitaxial 3C-SiC for MEMS application. *Mater. Sci. Forum* **679**, 133 (2011).
26. M. Zielinski, S. Ndiaye, T. Chassagne, S. Juillaguet, R. Lewandowska, M. Portail, A. Leycuras, and J. Camassel: Strain and wafer curvature of 3C-SiC films on silicon: Influence of the growth conditions. *Phys. Status Solidi A* **204**, 981 (2007).
27. A. Atkinson and S.C. Jain: Spatially resolved stress analysis using Raman spectroscopy. *J. Raman Spectrosc.* **30**, 885 (1999).
28. A. Severino, G. D'Arrigo, C. Bongiorno, S. Scalese, G. Foti, and F. La Via: Thin crystalline 3C-SiC layer growth through carbonization of differently oriented Si substrates. *J. Appl. Phys.* **102**, 023518 (2007).
29. Y. Sun. T. Miyasato, and N. Sonoda: Outdiffusion of the excess carbon in SiC films into Si substrate during film growth. *J. Appl. Phys.* **84**, 6451 (1998).
30. M. Bosi, G. Attolini, B.E. Watts, F. Rossi, C. Ferrari, F. Riesz, and L. Jiang: Evaluation of curvature and stress in 3C-SiC grown on differently oriented Si substrates. *J. Cryst. Growth* **318**, 401 (2011).
31. T. Chassagne, G. Ferro, H. Haas, H. Mank, A. Leycuras, Y. Monteil, F. Soares, C. Balloud, Ph. Arcade, C. Blanc, H. Peyre, S. Juillaguet, and J. Camassel: Control of 3C-SiC/Si wafer bending by the "checker-board" carbonization method. *Phys. Status Solidi A* **202**, 524 (2005).
32. J. Camassel: State of the art of 3C-SiC/silicon on insulators. *J. Vac. Sci. Technol, B* **16**, 1648 (1998).
33. C. Zgheib, L.E. McNeil, M. Kazan, P. Masri, F.M. Morales, O. Ambacher, and J. Pezoldt: Raman studies of Ge-promoted stress modulation in 3C–SiC grown on Si(111). *Appl. Phys. Lett.* **87**, 041905 (2005).
34. T. Chassagne, G. Ferro, C. Gourbeyre, M. Le Berre, D. Barbier, and Y. Monteil: Thermally induced surface reorganization of 3C-SiC (111) epilayers grown on silicon substrates. *Mater. Sci. Forum* **353**, 155 (2001).

https://doi.org/10.1557/jmr.2012.264 Published online by Cambridge University Press